Available online at www.sciencedirect.com
SCIENCE DIRECT®
Journal of Power Sources 119–121 (2003) 166–170
JOURNAL OF POWER SOURCES
www.elsevier.com/locate/jpowsour

Electrochemical performance of $Li[Li_xNi_{(1-3x)/2}Mn_{(1+x)/2}]O_2$ cathode materials synthesized by a sol–gel method

J.-H. Kim, Y.-K. Sun*

Department of Chemical Engineering, College of Engineering, Hanyang University, Seungdong-Gu, Seoul 133-791, South Korea

Abstract

Layered $Li[Li_xNi_{(1-3x)/2}Mn_{(1+x)/2}]O_2$ materials with $x = 0.05$, 0.1, 0.15, and 0.2 were synthesized using a sol–gel method. The layered $Li[Li_xNi_{(1-3x)/2}Mn_{(1+x)/2}]O_2$ structure was stabilized by a solid solution between $LiNiO_2$ and Li_2MnO_3. The discharge capacity of the $Li[Li_xNi_{(1-3x)/2}Mn_{(1+x)/2}]O_2$ electrodes increased with decreasing Ni content. $Li[Li_xNi_{(1-3x)/2}Mn_{(1+x)/2}]O_2$ electrode with $x = 0.05$, 0.1, 0.15, and 0.2 delivered high discharge capacities of 184, 193, 206, and 209 mAh g^{-1} at 30 °C, respectively, with excellent cycleability.

Keywords: Lithium secondary batteries; Sol–gel method; Layered manganese; Cathode materials; Li_2MnO_3

1. Introduction

$LiCoO_2$ has been commercialized as the active cathode material for lithium secondary batteries. Because of its toxicity and high cost, much effort has been made to find replacements such as lithium nickel oxides and lithium manganese oxides. Lithium nickel oxides are attractive materials for lithium secondary batteries. However, $LiNiO_2$ has some problems such as low discharge capacity (about 140–150 mAh g^{-1}) due to the difficulty in synthesis of stoichiometric $LiNiO_2$ and capacity degradation due to the formation of NiO_2 phase during intercalation/deintercalation of lithium ion [1]. Alternatively, lithium manganese oxides are less expensive and non-toxic than $LiCoO_2$ and $LiNiO_2$. Among them, $LiMn_2O_4$ has been received a great deal of attention for its easy preparation and low cost. However, $LiMn_2O_4$ shows serious problems such as Mn dissolution and large capacity loss at elevated temperature [2,3]. $LiMnO_2$ with the layered rock salt structure (α-$NaFeO_2$ type) was prepared by ion exchange of lithium salts with $NaMnO_2$ [4]. $LiMnO_2$ shows significant capacity fading and tend to transform to the more stable spinel phase during cycling due to the Jahn–Teller ions of Mn^{3+} [5–8].

Several recent studies have been focused on the solid solution between Li_2MnO_3 and $LiMO_2$ (M = Cr, Ni, Co) [9–12]. $Li_2M'O_3$ (M′ = Mn, Ti) has a layered structure similar to $LiCoO_2$, $LiNiO_2$, and $LiCrO_2$, however, it is an inactive material during the electrochemical charge–discharge process. This inactive Li_2MnO_3 component contributes to the structural stabilization of $LiMO_2$ (M = Cr, Ni, Co). $Li[Li_{(1/3-2x/3)}Ni_xMn_{(2/3-x/3)}]O_2$ is a solid solution of Li_2MnO_3 and $LiNiO_2$ [12].

In this paper, we report the synthetic method and electrochemical properties of $Li[Li_xNi_{(1-3x)/2}Mn_{(1+x)/2}]O_2$ ($x = 0.05$, 0.1, 0.15, and 0.2) materials synthesized using a sol–gel method.

2. Experimental

$Li[Li_xNi_{(1-3x)/2}Mn_{(1+x)/2}]O_2$ ($x = 0.05$, 0.1, 0.15, and 0.2) compounds were prepared by a sol–gel method using glycolic acid as a chelating agent. Stoichiometric amounts of $Li(CH_3COO)\cdot H_2O$, $Ni(CH_3COO)_2\cdot 4H_2O$, and $Mn(CH_3COO)_2\cdot 4H_2O$ were dissolved in distilled water. The dissolved solution was added dropwise to a continuously stirred aqueous solution of glycolic acid. The pH of the solution was adjusted to about 7.0–7.5 using ammonium hydroxide. The prepared solution was evaporated at 70–80 °C until a transparent sol and gel was obtained. The resulting gel precursor was decomposed at 480 °C for 5 h in air. The obtained material was ground and pressed into pellet. The pellet was calcined in air at 900 °C for 20 h and quenched to room temperature.

The powder X-ray diffraction (XRD, Rint-2000, Rigaku) measurement using Cu Kα radiation was employed to identify the crystalline phase of the synthesized material.

* Corresponding author. Tel.: +82-2-2290-0524; fax: +82-2-2282-7329.
E-mail address: yksun@hanyang.ac.kr (Y.-K. Sun).

0378-7753/03/$ – see front matter
doi:10.1016/S0378-7753(03)00172-1

Rietveld refinement was then performed on the X-ray diffraction data to obtain lattice constants.

Galvanostatic charge–discharge cycling was performed in a 2032-type coin cell. For the fabrication of the positive electrode, 20 mg of $Li[Li_xNi_{(1-3x)/2}Mn_{(1+x)/2}]O_2$ ($x = 0.05$, 0.1, 0.15, and 0.2) powder was mixed with 12 mg of conductive binder (8 mg of teflonized acetylene black and 4 mg of graphite). The mixture was pressed on 200 mm^2 stainless steel mesh used as the current collector and dried at 130 °C for 5 h in a vacuum oven. Lithium foil was used as the negative electrode. The electrolyte was 1 M $LiPF_6$ in a mixture of ethylene carbonate (EC) and dimethyl carbonate (DMC) (1:2 by volume).

3. Result and discussion

Fig. 1 shows the XRD patterns of $Li[Li_xNi_{(1-3x)/2}Mn_{(1+x)/2}]O_2$ ($x = 0.05$, 0.1, 0.15, and 0.2) powders with Miller indices indicated. All of the diffraction peaks can be indexed based on a hexagonal α-$NaFeO_2$ structure. The XRD patterns show that the prepared powders are well defined hexagonal layered structures. As can be seen in Fig. 1, diffraction peaks belonging to Li_2MnO_3 (monoclinic phase) at $2\theta = 20-25^\circ$ increase with increasing Li content, x, in $Li[Li_xNi_{(1-3x)/2}Mn_{(1+x)/2}]O_2$.

Fig. 2 shows that the lattice parameters a and c decrease, but the c/a ratio increases with increasing Li content, x, in $Li[Li_xNi_{(1-3x)/2}Mn_{(1+x)/2}]O_2$. This behavior indicates that Ni^{2+} ($r^{2+}_{Ni} = 0.69$ Å) is substituted for Li^+ ($r^{+}_{Li} = 0.76$ Å) and Mn^{4+} ($r^{4+}_{Mn} = 0.53$ Å) and a uniform solid solution is formed.

The initial charge–discharge profiles of the $Li[Li_xNi_{(1-3x)/2}Mn_{(1+x)/2}]O_2$ ($x = 0.05$, 0.1, 0.15, and 0.2) electrodes are shown in Fig. 3. The operating cut-off voltages for Li/$Li[Li_xNi_{(1-3x)/2}Mn_{(1+x)/2}]O_2$ ($x = 0.05$, 0.1, 0.15, and 0.2) cells were 2.5 and 4.6 V. In the first charge process, $Li[Li_xNi_{(1-3x)/2}Mn_{(1+x)/2}]O_2$ electrodes show a slope above 4.45 V. This suggests that Ni^{2+} is oxidized to Ni^{4+} during the portion of the charge to 4.45 V and that this is irreversible [12]. To confirm this indication, Li/$Li[Li_{0.1}Ni_{0.35}Mn_{0.55}]O_2$ cells were cycled between different voltage ranges. Fig. 4 shows the differential capacity versus voltage of the $Li[Li_{0.1}Ni_{0.35}Mn_{0.55}]O_2$ electrode in voltage ranges of 2.5–4.3, 2.5–4.4, and 2.5–4.5 V, respectively. It is observed that the irreversible capacity peak does not appear in the voltage range of 2.5–4.3 and 2.5–4.4 V. The irreversible peak appears only when the upper voltage limit is 4.5 V. From this result, we considered that irreversible capacity of Li/$Li[Li_xNi_{(1-3x)/2}Mn_{(1+x)/2}]O_2$ cell is formed in the 4.45 V region. In Fig. 3, it is observed that the average working discharge voltages of $Li[Li_xNi_{(1-3x)/2}Mn_{(1+x)/2}]O_2$ electrodes decline as the Ni content decreases. This behavior is also observed during subsequent charge–discharge cycles. The decline of the operating potential for $Li[Li_xNi_{(1-3x)/2}Mn_{(1+x)/2}]O_2$ electrodes means that both Ni and Mn participate in the redox reaction during the charge–discharge process. Lu et al. proposed that the capacity below about 3.5 V during discharge results from the reduction of Mn^{4+} to Mn^{3+} [12].

Fig. 5 shows the discharge capacity versus number of cycles for $Li[Li_{0.1}Ni_{0.35}Mn_{0.55}]O_2$ electrodes at different charge–discharge rates. For the electrode (electrode #1) cycled at 0.1 mA cm^{-2} initially, then 0.2 mA cm^{-2} (2 cycles), and finally, 0.4 mA cm^{-2}, a discharge capacity of 197 mA h g^{-1} was delivered at the 4th cycle, and then remained at 193 mA h g^{-1} after 37 cycles. Meanwhile, for the electrode (electrode #2) cycled at the constant current density of 0.4 mA cm^{-2} from the 1st cycle, an initial discharge capacity of 188 mA h g^{-1} was delivered, which increased steadily on subsequent cycles, and remained at 208 mA h g^{-1} after 37 cycles.

Fig. 6 shows the differential capacity versus voltage curves for the two $Li[Li_{0.1}Ni_{0.35}Mn_{0.55}]O_2$ electrodes at different charge–discharge rates. An oxidation peak above

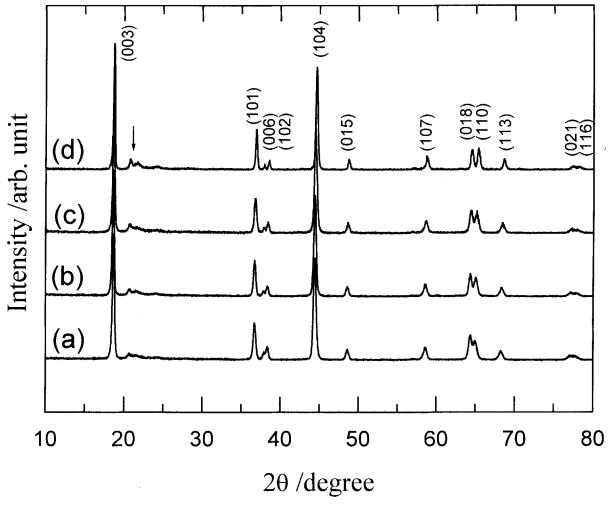

Fig. 1. X-ray diffraction patterns of $Li[Li_xNi_{(1-3x)/2}Mn_{(1+x)/2}]O_2$ powders. (a) $x = 0.05$, (b) $x = 0.1$, (c) $x = 0.15$, and (d) $x = 0.2$.

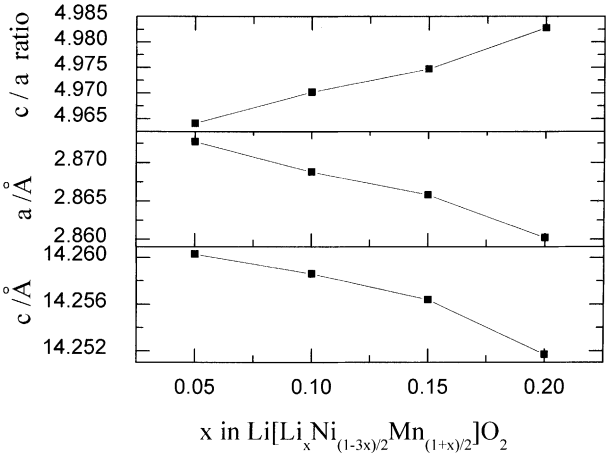

Fig. 2. Lattice constants a, c, and c/a ratio as a function of x in $Li[Li_xNi_{(1-3x)/2}Mn_{(1+x)/2}]O_2$.

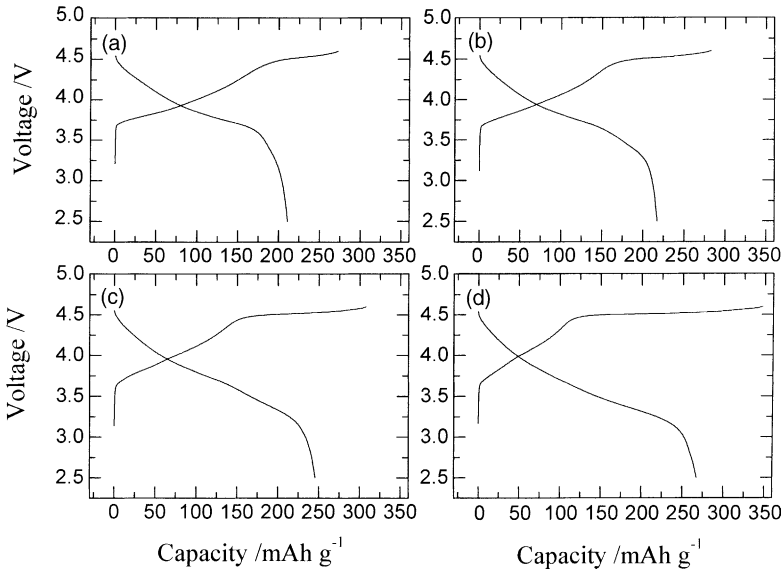

Fig. 3. The first charge–discharge curves of Li/Li[$Li_xNi_{(1-3x)/2}Mn_{(1+x)/2}$]$O_2$ electrodes at a rate of 0.1 mA cm^{-2} between 2.5 and 4.6 V. (a) $x = 0.05$, (b) $x = 0.1$, (c) $x = 0.15$, and (d) $x = 0.2$.

4.45 V appeared in the first charge, which is related to the irreversible capacity. In the case of electrode #1, there appeared a shoulder at about 3.2 V during discharge in the first cycle possibly due to a phase transition. Meanwhile, electrode #2 did not show the shoulder at about 3.2 V during the discharge process in the first cycle. The shoulder, however, started to develop and increased during the subsequent cycles. Additionally, an irreversible capacity peak above 4.45 V in the first charge process remained in the 2nd and 3rd cycle for electrode #2. Rapid growth of the shoulder near 3.2 V during discharge is believed to be the reason for the increased capacity of electrode #2. Meanwhile, in the case of electrode #1, the irreversible capacity peak was not observed after the first cycle. From these results, it is believed that the rate of lithium insertion and extraction at the current density of 0.4 mA cm^{-2} is too fast to complete the structural transition and the structural transition continues on the subsequent cycles. We speculate that the structural transition on the first 3 cycles resulted in increased displacement of the transition metal into the lithium layers, leading to lower capacity than that of the electrode cycled at the constant current density of 0.4 mA cm^{-2}.

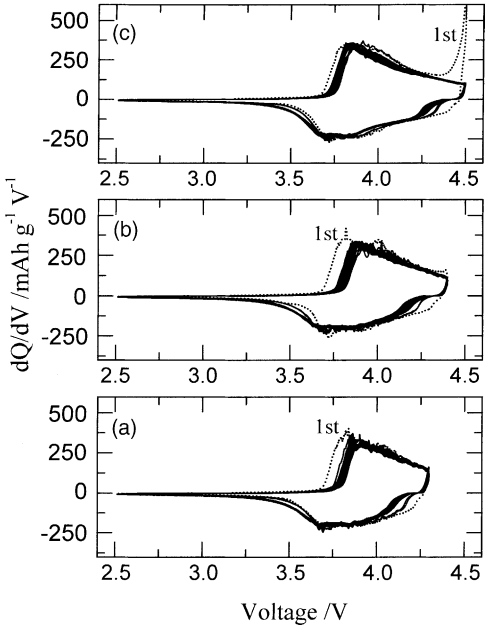

Fig. 4. dQ/dV vs. voltage of the Li[$Li_{0.1}Ni_{0.35}Mn_{0.55}$]$O_2$ electrodes over different voltage ranges. (a) 2.5–4.3 V, (b) 2.5–4.4 V, and (c) 2.5–4.5 V.

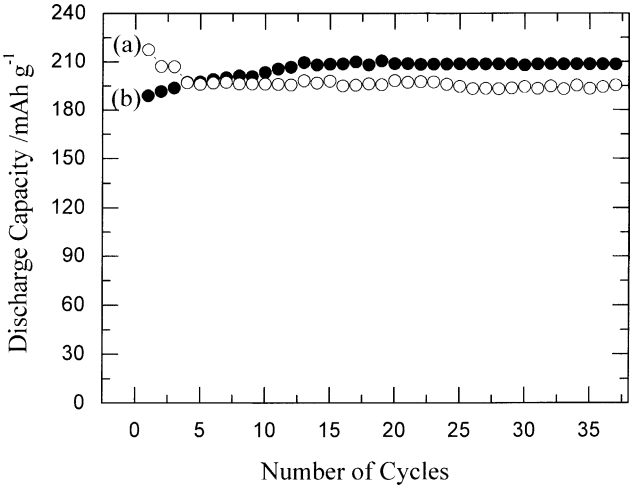

Fig. 5. The discharge capacity vs. number of cycles for Li[$Li_{0.1}Ni_{0.35}Mn_{0.55}$]$O_2$ electrodes at different charge–discharge rates at 30 °C. (a) 0.1 mA cm^{-2} initially, then 0.2 mA cm^{-2} (2 cycles), and finally 0.4 mA cm^{-2}, and (b) 0.4 mA cm^{-2}.

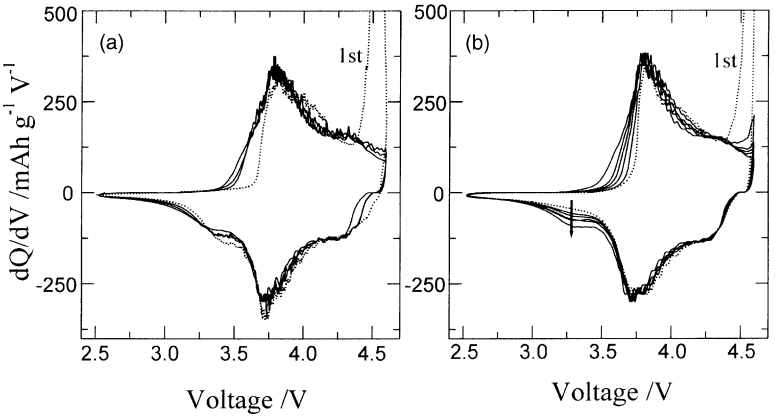

Fig. 6. The differential capacity vs. voltage of the $Li[Li_{0.1}Ni_{0.35}Mn_{0.55}]O_2$ electrodes at different charge–discharge rates at 30 °C. (a) 0.1 mA cm^{-2} initially, then 0.2 mA cm^{-2} (2 cycles), and finally 0.4 mA cm^{-2}, and (b) 0.4 mA cm^{-2}.

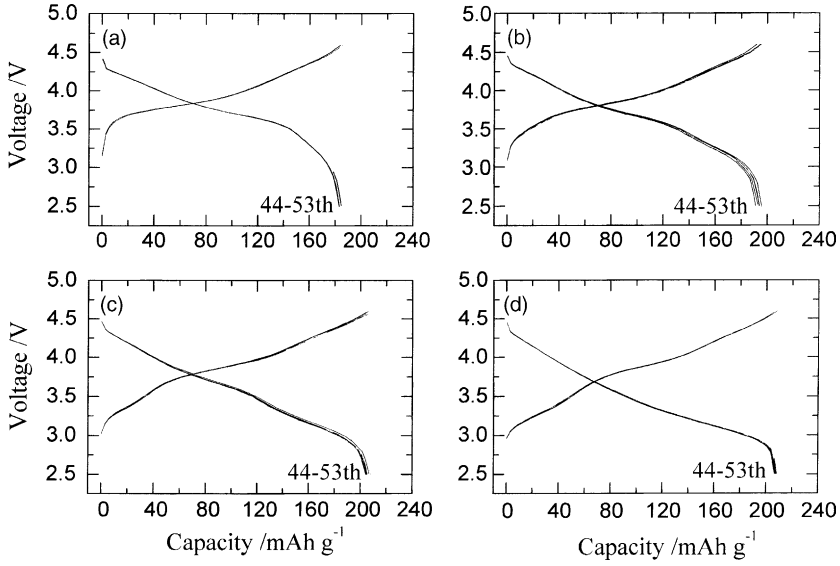

Fig. 7. Charge–discharge curves of the $Li[Li_xNi_{(1-3x)/2}Mn_{(1+x)/2}]O_2$ electrodes at a rate of 0.4 mA cm^{-2} between 2.5 and 4.6 V. (a) $x = 0.05$, (b) $x = 0.1$, (c) $x = 0.15$, and (d) $x = 0.2$.

Fig. 7 shows the voltage profiles of $Li/Li[Li_xNi_{(1-3x)/2}Mn_{(1+x)/2}]O_2$ ($x = 0.05$, 0.1, 0.15, and 0.2) cells for the 44th–53rd cycles between 2.5 and 4.6 V at 30 °C. All the electrodes exhibited similar results to the ones reported by other researchers [9–12].

Fig. 8 shows the specific discharge capacities versus the number of cycles for the $Li[Li_xNi_{(1-3x)/2}Mn_{(1+x)/2}]O_2$ ($x = 0.05$, 0.1, 0.15, and 0.2) electrodes between 2.5 and 4.6 V at 30 °C. All the electrodes except for $x = 0.2$ showed excellent cycleability. The $Li[Li_{0.2}Ni_{0.2}Mn_{0.6}]O_2$ electrode showed discharge capacity fading during the first 15 cycles, but the electrode retained its capacity well during subsequent cycles. It is suggested that the poor cycleability of $Li[Li_{0.2}Ni_{0.2}Mn_{0.6}]O_2$ electrode during the first 15 cycles is attributable to the migration of the transition metals into the lithium layer [12]. The $Li[Li_xNi_{(1-3x)/2}Mn_{(1+x)/2}]O_2$ electrodes with $x = 0.05$, 0.1, 0.15, and 0.2 after the 50 cycles provided specific discharge capacities of 184, 193, 206, and 209 mA h g^{-1}, respectively. Further studies are now in

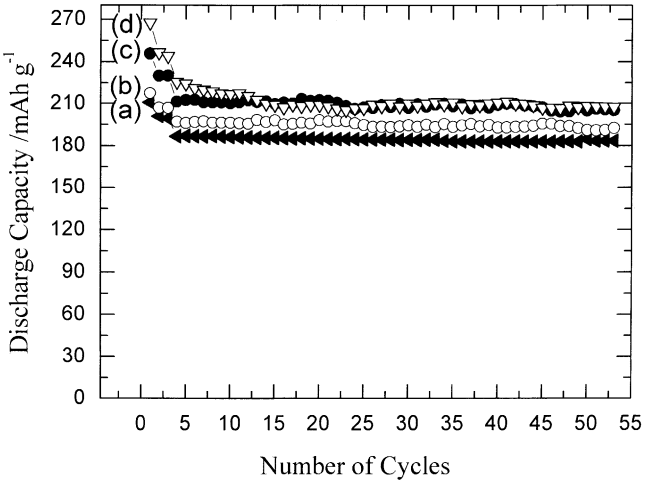

Fig. 8. The discharge capacity vs. number of cycles for the $Li[Li_xNi_{(1-3x)/2}Mn_{(1+x)/2}]O_2$ electrodes at a rate of 0.1 mA cm^{-2} initially, then 0.2 mA cm^{-2} (2 cycles), and finally 0.4 mA cm^{-2} (50 cycles) between 2.5 and 4.6 V. (a) $x = 0.05$, (b) $x = 0.1$, (c) $x = 0.15$, and (d) $x = 0.2$.

progress to reveal the structural transition of the $Li[Li_{(1-2x)/3}Ni_xMn_{(2-x)/3}]O_2$ materials.

4. Conclusions

The layered $Li[Li_xNi_{(1-3x)/2}Mn_{(1+x)/2}]O_2$ ($x = 0.05$, 0.1, 0.15, and 0.2) powders with excellent homogeneity and crystallinity have been synthesized using a sol–gel method. The layered structure was obtained by forming a solid solution through Ni substitution into the Li and Mn sites in Li_2MnO_3 structure. The electrochemically inactive Li_2MnO_3 component contributes to stabilization of the $Li[Li_xNi_{(1-3x)/2}Mn_{(1+x)/2}]O_2$ host structure.

Acknowledgements

This work is supported in part by the Ministry of Information & Communication of Korea (“Support Project of University Information Technology Research Center” supervised by KIPA).

References

[1] T. Ohzuku, A. Ueda, M. Nagayama, J. Electrochem. Soc. 140 (1993) 1563.
[2] G.G. Amatucci, C.N. Schmutz, A. Bylr, C. Siala, A.S. Gozdz, D. Larcher, J.M. Tarascon, J. Power Sources 69 (1997) 11.
[3] Y.K. Sun, D.W. Kim, Y.M. Choi, J. Power sources 79 (1999) 231.
[4] A.R. Armstrong, P.G. Bruce, Nature 381 (1996) 499.
[5] Y. Shao-Horn, S.A. Hackney, A.R. Armstrong, P.G. Bruce, R. Gitzendanner, C.S. Johnson, M.M. Thackeray, J. Electrochem. Soc. 146 (1999) 2404.
[6] A.R. Armstrong, R. Gitzendanner, A.D. Robertson, P.G. Bruce, Chem. Commun. (1988) 1833.
[7] Y.I. Jang, B. Huang, Y.M. Chiang, D.R. Sadoway, Electrochem. Solid-State Lett. 1 (1998) 13.
[8] B. Ammundsen, J. Desilvestro, T. Groutso, D. Hassell, J.B. Metson, E. Regan, R. Steiner, P.J. Pickering, J. Electrochem. Soc. 147 (2000) 4078.
[9] K. Numata, C. Sakaki, S. Yamanaka, Solid State Ionics 117 (1999) 257.
[10] B. Ammundsen, J. Desilvestro, R. Steiner, P. Pickering, in: Proceedings of the 10th International Meeting on Lithium Batteries, vol. 97–98, Como, Italy, 28 May–2 June 2000.
[11] T. Ohzuku, Y. Makimura, Chem. Lett. (2001) 744.
[12] Z. Lu, J.R. Dahn, J. Electrochem. Soc. 149 (2002) A815.